Structure and Velocity of the Periodic Vortex-Ring Flow Pattern of a Primary Pfeifenton (Pipe Tone) Jet

A. B. C. Anderson

Citation: The Journal of the Acoustical Society of America **27**, 1048 (1955); doi: 10.1121/1.1908112
View online: https://doi.org/10.1121/1.1908112
View Table of Contents: http://asa.scitation.org/toc/jas/27/6
Published by the Acoustical Society of America

Structure and Velocity of the Periodic Vortex-Ring Flow Pattern of a *Primary Pfeifenton* (Pipe Tone) Jet

A. B. C. ANDERSON
Michelson Laboratory, U. S. Naval Ordnance Test Station, Inyokern, China Lake, California
(Received April 25, 1955)

Visualization of the vortex flow pattern in typical *primary Pfeifenton* jets was made by means of shadowgraph techniques to show the transition in form of the vortex pattern as it moves downstream in the jet, as well as, the dependence of the downstream translational vortex velocity and the geometry of the vortex pattern on the Reynolds number of the jet.

Results of experiment are compared with available theory. These studies were carried out with carbon dioxide jets discharging into the atmosphere. The flow channel geometry consisted of a pipe $\frac{7}{8}$ in. in diameter, 12.013 in. long effectively, open at one end which was inserted into a large stilling tank and terminated at the other end by an orifice plate containing a sharp-edged circular orifice, 0.250 in. in diameter and 0.093 in. thick.

INTRODUCTION

As Reynolds number Re of the flow through a circular sharp-edged orifice terminating a pipe (resonant-chamber orifice combination) is gradually changed, discrete ranges of self-excited eigenfrequencies, *Pfeifentöne,* are produced inside the pipe.[1,2] The *primary Pfeifenton* frequency is the one associated with the low Re end of each of the discrete ranges of pipe tones.

Experimental evidence,[1–3] including that to be presented here, supports the view that the mechanism for excitation of the *Pfeifentöne* may be periodic fluctuations of the effective aerodynamic orifice area produced by the growth and periodic shedding of vortices (the boundary layer) from side walls of the orifice. Fluctuation of effective orifice area would then create periodic fluctuations in discharge rate and, therefore, fluctuations in pressure inside the pipe in the vicinity of the orifice. These periodic pulses propagate upstream in the pipe. If the frequency of the pulses is equal to or a multiple of one of the resonant eigenfrequencies of the pipe-orifice combination, the column of gas in the pipe sings out especially clearly to give a pronounced *Pfeifenton.*

Associated with the *Pfeifenton* is a jet, emerging from the orifice, composed of a periodic arrangement of vortex rings. As first shown by Kelvin,[4] the axial velocity of translation v of an isolated vortex ring in a perfect fluid is

$$v=\frac{k}{4\pi R}\left[\ln\left(8\frac{R}{r}\right)-\frac{1}{4}\right],$$

where the radius r of the circular cross section (core) of vortex has been assumed small compared with ring radius R, and where k is the strength of the whole vortex.

Considerations leading to the development of this expression lead to the deduction that if a number of vortex rings co-exist, each ring will move without sensible change of shape or size and with nearly uniform velocity in the direction of its rectilinear axis until it comes within a short distance of a second ring. If the two circular vortices have the same rectilinear axis and the same sense of rotation, the two rings will advance in the same direction. Owing to their interaction, the ring radius of the downstream vortex will increase causing its axial velocity of translation to decrease; the ring radius of the upstream vortex will decrease causing its axial velocity of translation to increase. It may, therefore, happen that the upstream vortex ring will overtake and pass through the downstream ring.

Studies have been made indicating that the foregoing expression is helpful in explaining the nature of the downstream movement of liquid vortices generated at the sharp-edged entrance of a circular pipe.[5] The quantities v, r, and R were evaluated from the flow pattern of colored liquid tracer filaments injected upstream by a hypodermic needle. The vortices, and therefore the circulation in the vortices, appeared to be generated in the *Totwasser* space between the *vena contracta* and the tube walls at the tube entrance. They were formed by the rolling up of lengths of transition layer[6–9] assumed equal to the vortex separation l.

For laminar flow this leads to vortices of core radius r having a circumference $l=2\pi r$. Circumferential velocity of the vortices was assumed to be $\bar{u}/\alpha$ where $\bar{u}$ is the mean velocity of flow in the pipe and α is the contraction area ratio at the *vena contracta* (cross section of the *vena contracta* divided by the pipe cross section). Therefore, the strength of each vortex $k=2\pi r(\bar{u}/\alpha)=l(\bar{u}/\alpha)$ all quantities of which are experimentally measurable. The resultant vortex strength of a downstream vortex resulting from the coalescence of two or more of these was considered equal to the sum of the component strengths.

[1] A. B. C. Anderson, J. Acoust. Soc. Am. **25**, 541–545 (1953).
[2] A. B. C. Anderson, J. Acoust. Soc. Am. **24**, 675–681 (1952).
[3] A. B. C. Anderson, J. Acoust. Soc. Am. **25**, 626–631 (1953).
[4] Horace Lamb, *Hydrodynamics* (Dover Publications, New York, 1945), pp. 241, 242.
[5] Hermann Kurzweg, Ann. Physik **18**, 193–216 (1933).
[6] L. Schiller, 3. Intern. Kongr. Tech. Mech. Teil **I**, 226–233, Stockholm (1931).
[7] A. Naumann, Forsch. Gebiete Ingenieurw. **2**, 85–98 (1931).
[8] H. Hahnemann, Forsch. Gebiete Ingenieurw. **8**, 226–237 (1937).
[9] A. B. C. Anderson, J. Acoust. Soc. Am. **27**, 13 (1955).

For turbulent flow downstream in the pipe, larger and more well-defined vortices were observed in the *Totwasser* space. Observation suggested that the diameter of these vortices should be taken as equal to the distance $2r=(d/2)(1-\sqrt{\alpha})$ between the *vena contracta* and the pipe wall,[6,7] where d is the internal pipe diameter. The circumferential velocity around the vortex was again assumed $\bar{u}/\alpha$, so that the vortex strength is now $k=\pi\bar{u}d(1-\sqrt{\alpha})/2\alpha$.

Kelvin's expression has also been used with apparent success[10,11] to account for some of the behavior of vortices in a jet where, again, the vortex strength k of each vortex was taken as $(\bar{u}/\alpha)l$. Associated with this was also the deduction that vortex separation, orifice diameter and vortex-ring diameter should be approximately equal to each other. On the other hand, an analysis has also been made to show that there should exist no stable value for the ratio of vortex-ring diameter to vortex-ring separation,[12] as in the case of the Kármán vortex street.[13]

A vital distinction exists between interaction of separate vortices in a perfect fluid and interaction of separate vortices in a viscous fluid.[14] In the former, the vortices during their interplay will always retain their separate identities regardless of their relative strengths and signs. In the latter, experiment shows that a vortex may change in intensity by directly absorbing any number of others, the system coalescing into one or more distinct vortices, while at the same time their combined energies degrade gradually into heat.

The present paper is concerned with visualization of the vortex-flow pattern in typical *primary Pfeifenton* jets by means of shadowgraph techniques, the transition in form of the pattern as it moves downstream, and the dependence of the downstream translational vortex velocity on Re of the jet.

APPARATUS

These studies were carried out with carbon dioxide jets discharging into the atmosphere. The flow channel geometry consisted of a pipe $\frac{7}{8}$ in. in diameter, 12.013 in. long effectively, open at one end which was inserted into a large stilling tank, and terminated at the other end by an orifice plate containing a sharp-edged circular orifice, 0.250 in. in diameter and 0.093 in. thick. The equipment was the same as described elsewhere,[1,2] except for the shadowgraph arrangement shown schematically, Fig. 1.

To obtain successive pictures of the same jet, and therefore, to observe the transition in form of the jet vortex pattern with elapse of time, two sparks S_1 and S_2[15] were mounted as in Fig. 1. After S_1 discharged producing an image of jet J on one-half of film F, S_2 discharged at a suitable predetermined time later producing a second image of jet J on the other half of the same film F. Knife edges E_1 and E_2 define the borders of the two shadowgraph pictures. A part of the stroboscopic wheel W, having equally spaced holes punched around its periphery and rotating at a known constant velocity, was placed so that part of it shaded film F and was coplanar with it. The dot separation, produced photographically by the holes on the shadowgraphs, permitted a direct determination of the time interval between the two shadowgraph exposures.

Measurements on the shadowgraphs were greatly facilitated by the use of a Universal Telereader Type 17-A developed by the Telecomputor Corporation, Burbank, California. An expression of appreciation to Dr. A. G. Hoyem and W. C. Ward of the Aviation Ordnance Department for having made this instrument available is hereby acknowledged; also appreciation is extended to Dr. George Kretschmar and Leo Phegley for development and perfection of the timing and triggering circuits.

EXPERIMENTAL RESULTS

Figures 2 to 8 show typical side views of the periodic vortex-ring structure observed. The jets are all discharging upward from the orifice located at the bottom of each shadowgraph. The shadowgraphs occur in pairs, the right-hand showing the jet at a slightly later time then the left.

The time interval between the two shadowgraphs of a pair is determined from the separation of two sets of dots at the top of each pair produced by the stroboscope wheel W, Fig. 1. These are shown only at top of Fig. 2, having been blanked off from the other figures for economy of space. This time interval at the principle sound frequency observed in the resonant cavity and other related data, are shown in the legends. The numbers in parentheses denote the laboratory notebook number of the shadowgraph picture. The length scale used in evaluating the geometry of each pair of shadowgraphs is given by the separation (0.500 cm) of the notches on the posts on each side of each pair of shadowgraphs.

Most of the shadowgraphs show vortex coalescence. Figure 2 shows pairs of vortices of seemingly equal strength coalescing downstream. The original photographs are much clearer and show far more detail. Figures 3 and 4 show two successive stages in the coalescence of a small amplitude second harmonic vortex near orifice with a large amplitude vortex a bit farther *upstream*. Figures 5 and 6, on the other

[10] Henning von Gierke, "Über schneidentöne an kreisrunden gasstrahlen und ebenen lamellen," dissertation, Technischen Hochschule Karlsruhe (1944).
[11] Henning von Gierke, Z. angew. Phys. 2, 97–106 (1950).
[12] H. Levy and A. G. Forsdyke, Proc. Roy. Soc. (London) A114, 594–604 (1927).
[13] Th. v. Kármán, Gessellschaft Wiss. Göttingen 5, 547–556 (1911–1912).
[14] H. Levy, Phil. Mag. 2, 844–851 (1926).
[15] Frank N. Miller, "A short-duration collimated light source," US NOTS, Inyokern NAVORD Rept. 3350, July 16, 1954.

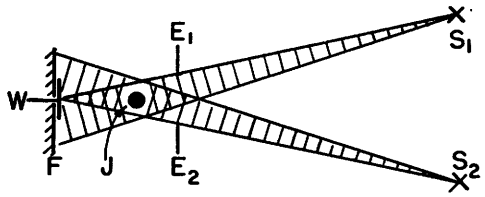

FIG. 1. Shadowgraph arrangement.

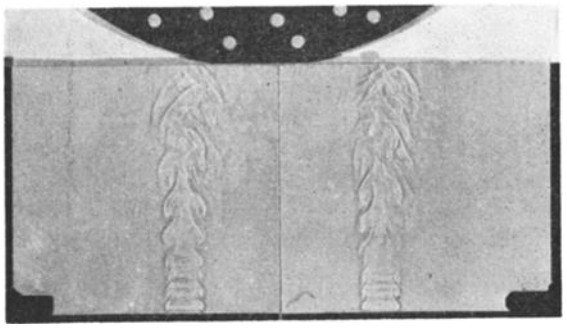

FIG. 2. $f=756.5$ cps, Re $=583$, $\Delta t=1.17\times10^{-3}$ sec (497).

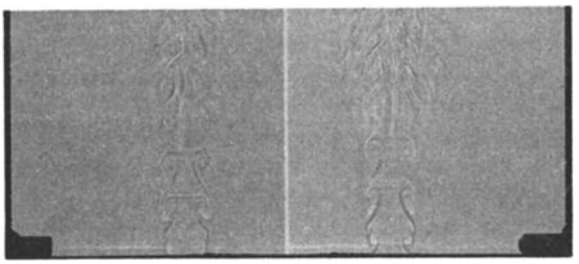

FIG. 3. $f=362$ cps, Re $=738$, $\Delta t=0.889\times10^{-3}$ sec (787).

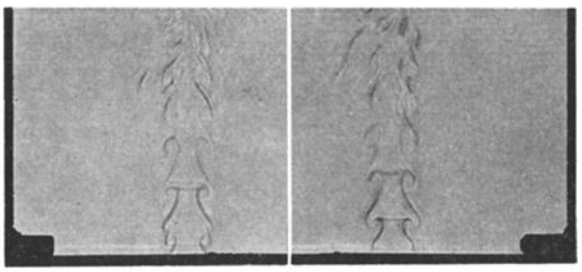

FIG. 4. $f=362$ cps, Re $=738$, $\Delta t=0.889\times10^{-3}$ sec (789).

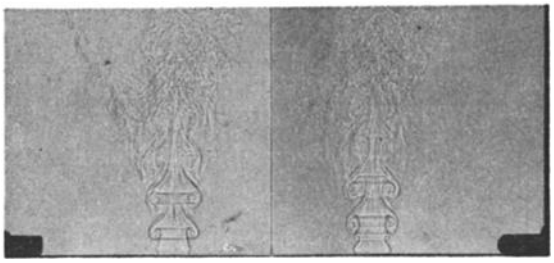

FIG. 5. $f=1595$ cps, Re $=3196$, $\Delta t=0.186\times10^{-3}$ sec (551).

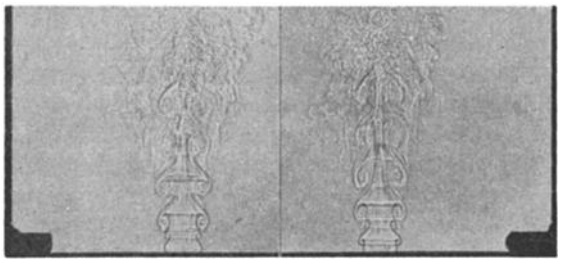

FIG. 6. $f=1595$ cps, Re $=3196$, $\Delta t=0.186\times10^{-3}$ sec (553).

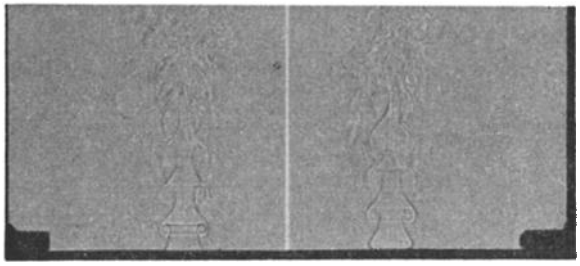

FIG. 7. $f=745$ cps, Re $=1355$, $\Delta t=0.565\times10^{-3}$ sec (900).

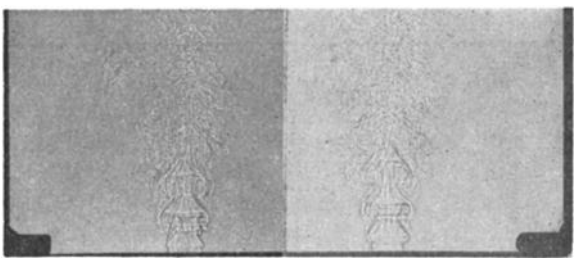

FIG. 8. $f=2498$ cps, Re $=4348$, $\Delta t=0.139\times10^{-3}$ sec (956).

FIGS. 1–8. Shadowgraph arrangement and typical side views of the periodic vortex ring structure observed. Jets are all discharging upward from the orifice located at bottom of each shadowgraph. The shadowgraphs occur in pairs, the right-hand showing the jet at a slightly later time Δt than the left. The length scale used in evaluating the geometry of each pair of shadowgraphs is given by the separation (0.500 cm) of the notches on the posts on each side of each pair of shadowgraphs. Number in parentheses denotes laboratory notebook number of the shadowgraph picture.

hand, show two successive stages in the coalescence of a small amplitude second harmonic vortex near orifice with a large amplitude vortex a bit farther *downstream*. In one case, Figs. 3 and 4, a resultant attraction appears between a small vortex ring and a large one *upstream*; in the other case, Figs. 5 and 6, a resultant attraction appears between a small vortex ring and a large one *upstream*; in the other case, Figs. 5 and 6, a resultant attraction appears between a small vortex ring and a large one *downstream*.

Figure 8 also illustrates vortex coalescence. A combination of vortices in the left shadowgraph, just above the orifice, coalesce into a larger more organized single vortex on the right.

Generally, during the close approach of two or more vortices, the following occurs entailing vortex coalescence: The downstream vortex expands and slows down; the upstream contracts and speeds up, finally to overtake and coalesce with the downstream vortex. This behavior is to be expected from a consideration of the interaction of the fields of circulation about the vortices. Frequently, especially when vortex coalescence

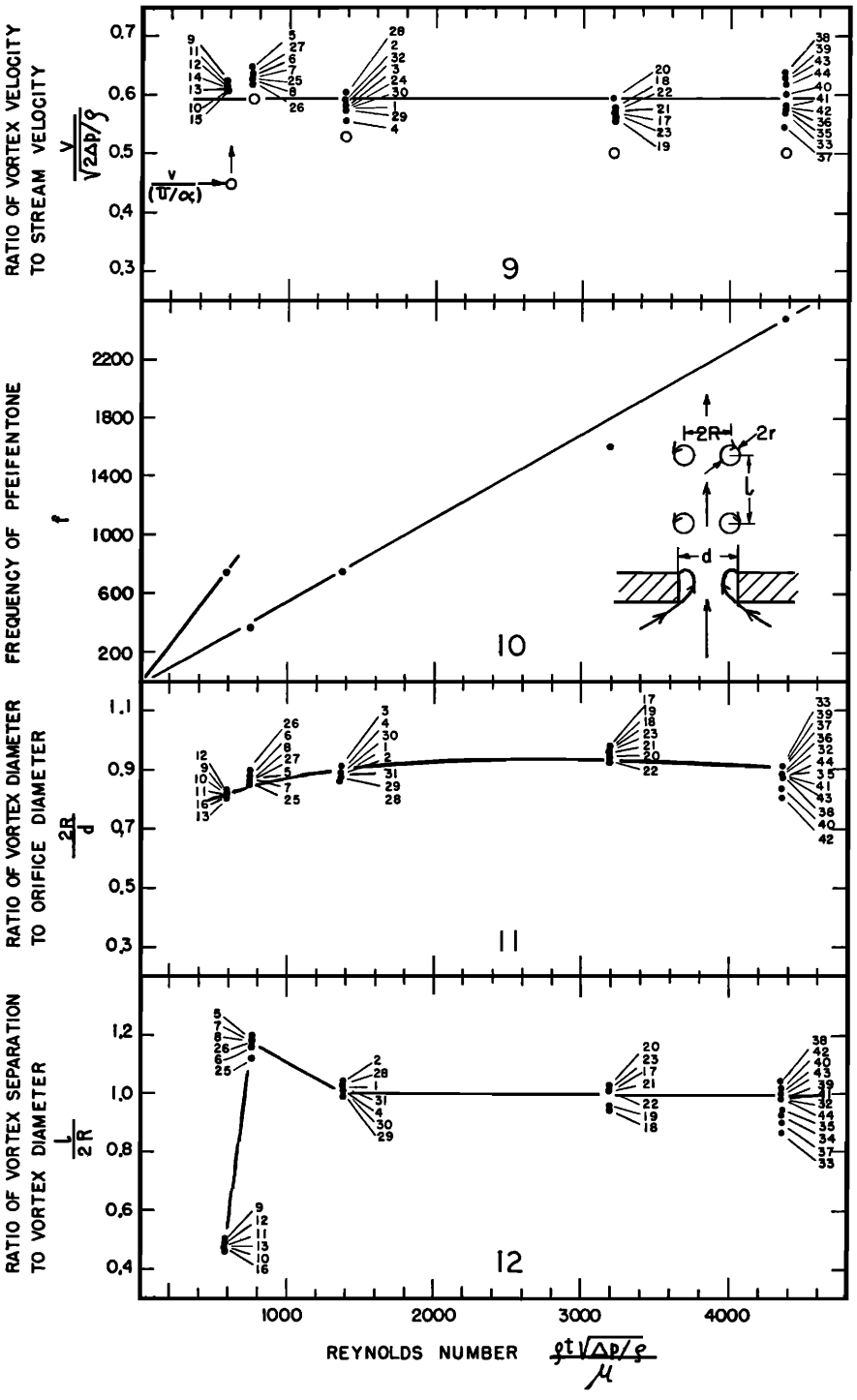

FIG. 9. Experimental dependence of ratio $v/(2\Delta p/\rho)^{\frac{1}{2}}$ [of vortex velocity v in jet to the jet stream velocity expressed as $(2\Delta p/\rho)^{\frac{1}{2}}$, where Δp is the pressure across the orifice and ρ is gas density] on Re of jet (expressed as $\rho t(\Delta p/\rho)^{\frac{1}{2}}/\mu$ where t is thickness of orifice plate and μ viscosity of gas). Large hollow circles show the theoretical dependence of $v/(\bar{u}/\alpha)$ on Re, where $\bar{u}$ is mean velocity of flow through orifice and α is contraction area ratio of flow at *vena contracta*.

FIG. 10. Dependence of *primary Pfeifenton* frequency f on Re. Deviation of point at Re = 3196 from straight line due to fact that this jet was a little above the *primary Pfeifenton* condition. This in no way, however, invalidates the results in Figs. 9, 11, and 12. Diagram at right serves to define terms used in the geometrical description of vortex train.

FIG. 11. Dependence of ratio $2R/d$, of vortex diameter $2R$ to orifice diameter d, on Re.

FIG. 12. Dependence of ratio $l/2R$, of vortex separation l to vortex diameter $2R$, on Re. Numbers attached to points denote the laboratory notebook number of the shadowgraph picture according to following code:

1, 393; 2, 394; 3, 395; 4, 396; 5, 411; 6, 412; 7, 413; 8, 414; 9, 485; 10, 486; 11, 491; 12, 492; 13, 495; 14, 496; 15, 497; 16, 498; 17, 550; 18, 553; 19, 555; 20, 556; 21, 564; 22, 565; 23, 566; 24, 586; 25, 774; 26, 780; 27, 788; 28, 900; 29, 901; 30, 906; 31, 907; 32, 908; 33, 948; 34, 922; 35, 949; 36, 950; 37, 953; 38, 955; 39, 956; 40, 960; 41, 962; 42, 963; 43, 964; 44, 965.

is not significant, as in Fig. 7, the jet vortices continue to move downstream very evenly without appreciable change of shape, separation, or translational velocity.

Calculation of the vortex shedding frequency from the displacement of the vortices in each pair of shadowgraphs always showed that the shedding frequency of the largest vortices equaled the frequency of the tone of largest amplitude recorded by the sound pickup.

Figure 9 presents the ratio $v/[2\Delta p/\rho]^{\frac{1}{2}}$, of the vortex velocity in the jet to the jet stream velocity u [expressed as $[2\Delta p/\rho]^{\frac{1}{2}}$, where Δp is pressure difference across the orifice and ρ is the gas density] as a function of Re of the jet [expressed as $\rho t(\Delta p/\rho)^{\frac{1}{2}}/\mu$, where t is thickness of orifice plate and μ viscosity of gas].[1,2] These ratios were determined from a number of shadowgraphs of which Figs. 2 to 8 are typical. Within

experimental scattering the ratio appears fairly independent of Re even though the frequency of the principal tone inside the resonant cavity and the rate of shedding of the vortices downstream from the orifice vary over the wide range shown in Fig. 10. Variation of the jet stream velocity $(2\Delta p/\rho)^{\frac{1}{2}}$ with change of Re also parallels Fig. 10 since the orifice number $tf/(\Delta p/\rho)^{\frac{1}{2}}$ has been shown to be relatively constant[16] where f is pipetone frequency.

All the *primary Pfeifentöne* observed, with the pipe-orifice combination used in this study, are presented in this paper except the one around 1150 cps. This one has been omitted because of its different and very unusual vortex flow pattern which showed an amazing and reproducible splitting of the jet (upon emergence from the orifice) into *two distinct circular vortex trains*. The axes of these vortex trains made a considerable angle with respect to the normal to the orifice plate. The two trains always lay in a plane passing through the normal to the plate. The geometrical form of the forked vortex train may be described by the fact that *alternate* vortices emerging from the orifice were always thrown into one and the same branch of the forked train. Details on this will be presented in a later paper.

Figure 11 shows the ratio $(2R/d)$ of vortex diameter to orifice diameter as a function of Re. These terms are defined as indicated schematically in Fig. 10. In general, vortex diameter is a bit smaller than orifice diameter and is relatively constant with change of Re.

Figure 11 also gives the mean calculated values of the ratio (R/r), of vortex ring radius to vortex core radius for the different pipe tones. This ratio is involved in the Kelvin expression for vortex-ring translational velocity. Some arbitrariness is of necessity involved in the definition and experimental determination of the vortex core radius r from the shadowgraphs. All the visible cross section in the shadowgraph associated with a vortex was not assumed to be vortex core, only the part enclosed by the dark innermost ring or arc of each vortex cross section. Inside this ring, the photographic darkening of the shadowgraph appears relatively uniform. This is clearly visible in all originals of shadowgraphs, Figs. 3 to 8. In Fig. 2, the position of the dark ring, however, could only be estimated from the position of the relatively white ring that usually accompanies and partly surrounds the dark ring. Absence of any visible appearance of the dark ring, Fig. 2, and not in the others, is not unreasonable because the derivative of the gas density gradient (which determines photographic contrast in a shadowgraph) across the vortex cores of this pipe tone jet should be less than for any of the others.

Figure 12 shows the ratio $(l/2R)$, of vortex separation to vortex-ring diameter as function of Re. The means of this ratio for the different pipe tones are not all equal and neither are they always approximately equal to unity. The latter appears at variance with conclusions deduced theoretically elsewhere[10,11] which seem to conclude that one should find $l/2R \approx 1$.

DISCUSSION

Kelvin's expression for vortex translational velocity was derived for a free and isolated vortex. For a train of circular vortices such as found in the present studies, the expression would seem most appropriate for vortices least involved in vortex coalescence, that is, where the vortex-ring diameter $2R$ and vortex separation l of the different vortices remain relatively constant with elapse of time as the vortices move downstream. This appears true in Fig. 7, in the downstream part of Figs. 3, 4, 5, 6, 8, and possibly to some extent in the upstream part of Fig. 2.

The expression would seem least appropriate where the vortices are close enough so that their interaction leads rather quickly to vortex coalescence. In this case, when two vortices are in the process of coalescing, the vortex diameter of the downstream vortex increases while its vortex velocity decreases; the diameter of the upstream vortex decreases while its vortex velocity increases. This appears especially true in the upstream parts of Figs. 3, 4, 5, 6, 8 and possibly, to some extent, in the upstream part of Fig. 2.

In this paper, also, let it be assumed[5–8,10,11] that the vortex strength $k=l(\bar{u}/\alpha)$. This expression may be justified in the present case on the basis that the circulation generated per second in the jet transition boundary layer is $kf=v(\bar{u}/\alpha)$. Since $v=lf$, the circulation generated per second becomes $lf\bar{u}/\alpha$, and therefore the circulation generated per vortex (vortex strength) is $k=l\bar{u}/\alpha$. Substituting this into Kelvin's expression, as well as the appropriate experimental values of $l/2R$ and R/r obtained from Figs. 11 and 12 and listed in Table I, gives the values of the vortex translational velocity in the last column, Table I, expressed in the form $v/[\bar{u}\alpha]$. These values are indicated in Fig. 9 by large hollow circles.

Insofar as $\bar{u}/\alpha$ (the jet stream velocity through the *vena contracta*) equals $(2\Delta p/\rho)^{\frac{1}{2}}$ (the jet stream velocity according to the Bernoulli equation) Fig. 9 gives a comparison of experimental and theoretical values of vortex velocity expressed in terms of stream velocity.

It is somewhat difficult to make a meaningful numerical comparison between values of $v/(2\Delta p/\rho)^{\frac{1}{2}}$ obtained here for pipe tones and values of $v/\bar{u}$ obtained elsewhere[10,11] for jet tones because of the different measures of stream velocity used in the two studies.

The two sets of values are comparable, however. Visualization of vortices in the latter study was accomplished by adding white ammonium chloride smoke upstream of the jet and viewing the jet with a stroboscope.

Although the experimental values of the velocity ratio appear to fall somewhat above the theoretical,

[16] A. B. C. Anderson, J. Acoust. Soc. Am. **26**, 21–25 (1954).

Fig. 9, the trend in the ratio, with change of Re, appears the same in both. According to the convention for determining vortex-core radius r adopted and described earlier, only in the case of the vortices obtained at Re 583 was there any great indecision as to the proper value to take for vortex core diameter. For more precise determinations of the vortex velocity ratio than possible here, it would be desirable to know how the velocity distribution across the jet (in the orifice and a bit downstream from the orifice) varies with Re, how closely the appropriate velocity in the expression for the strength k of the vortices agrees with $(2\Delta p/\rho)^{\frac{1}{2}}$, and to have a better understanding of the relation between what is seen photographically in the shadowgraph of a vortex and the velocity and density distribution in the vortex.

Figure 12 indicates there is no one single preferred vortex separation l for vortices just emerging from the circular orifice. This appears somewhat at variance with other studies[10,11] which seem to conclude that one should find $l \approx 2R$. The other studies, however, appear to have been carried out on jet tones from circular orifices generally having $t/d \approx 1$. Figures 2 to 8 indicate, nevertheless, that vortices in a circular vortex train whose $l/2R \ll 1$ prefer and endeavor to coalesce downstream into a train whose $l/2R$ is considerably greater.

TABLE 1.

Primary *Pfeifenton* frequency f	Ratio of vortex separation to vortex diameter $l/2R$	Ratio of vortex-ring radius to vortex core radius R/r	Reynolds numbers Re	Calculated ratio of vortex translational velocity to jet velocity through *vena contracta* $\frac{v}{\bar{u}/\alpha}$
756	0.485	50 or greater	583	0.45
362	1.19	3.51	738	0.58
745	1.00	4.37	1378	0.53
1595	0.99	3.87	3196	0.50
2490	0.985	3.80	4348	0.50

This increased tendency towards instability and vortex coalescence of vortices in a vortex train having $l/2R \ll 1$ may result from the greater degree of interaction existing between vortices that are closer together, superimposed on any inequalities in the strength and relative separation of the vortices leaving the orifice.

Although Figs. 2 to 8 and 12 might lead one to infer that all circular vortex trains tend to approach $l/2R \approx 1$ before dissolution by viscosity, this broad generalization is not considered substantiated here. An analysis has been made elsewhere to show that there exists no stable value for the ratio $l/2R$ of a circular vortex train as exists for the Kármán street.[13]